Symmetries and entanglement features of inner-mode-resolved correlations of interfering nonidentical photons

Simon Laibacher and Vincenzo Tamma

Phys. Rev. A **98**, 053829 — Published 19 November 2018

DOI: 10.1103/PhysRevA.98.053829

Symmetries and entanglement features of inner-mode resolved correlations of interfering nonidentical photons

Simon Laibacher[1] and Vincenzo Tamma[2,3,1,*]

[1] *Institut für Quantenphysik and Center for Integrated Quantum Science and Technology (IQ^{ST}), Universität Ulm, D-89069 Ulm, Germany*
[2] *School of Mathematics and Physics, University of Portsmouth, Portsmouth PO1 3QL, UK*
[3] *Institute of Cosmology & Gravitation, University of Portsmouth, Portsmouth PO1 3FX, UK*

Multiphoton quantum interference underpins fundamental tests of quantum mechanics and quantum technologies. Consequently, the detrimental effect of photon distinguishability in multiphoton interference experiments can be catastrophic. Here, we employ correlation measurements in the photonic inner modes, time or frequency, to restore quantum interference between photons differing in their colors or injection times in arbitrary linear optical networks, without the need for additional filtering or post selection. Interestingly, we demonstrate how harnessing the multiphoton inner-mode quantum information enables to infer information about symmetries of multiphoton networks and states and to observe arbitrary degrees of W-state entanglement between a small number of photons with a fixed interferometer. These results are therefore of profound interest for future applications of universal inner-mode resolved linear optics across fundamental science and quantum technologies with photons with experimentally different spectral properties.

I. INTRODUCTION AND MOTIVATION

The nonclassical interference of light [1–3] is one of the main consequences of the quantum nature of the electromagnetic field and lies at the heart of many quantum optics experiments [1–14]. It plays a central role in a variety of applications ranging from quantum computing [4, 15–19] over quantum communication and quantum cryptography [20, 21] to quantum metrology and state tomography [9–12, 14, 22–24]. Conventional multiphoton experiments in linear interferometers rely on measurements at the interferometer output which do not resolve the structure of the multiphoton interference in the photonic spectral degrees of freedom, namely frequency and time, effectively ignoring the full quantum information encoded in the photonic spectra. This "ignorance" can lead to the degradation of the observed multiphoton interference with increasing distinguishability for photons with nonidentical input states [5]. This is indeed the case for single-photon emitters, such as diamond colour centers [25], single molecules [26] and quantum dots [27, 28]. Here, photons emitted by different sources or by the same source at different times are generally different in their spectra.

Fortunately, with the advent of detectors with unprecedented time- or frequency-resolution, linear optical correlation experiments based on inner-mode resolving measurements either in time or frequency have become feasible [29–36]. As a result, full multiphoton interference can be observed at the output of a linear network even in the case of nonidentical input photons [5, 29]. Additionally, the dependence of the correlations of three photons at the output of a linear network has been investigated as a function of the spectral overlap of the input photons [37, 38].

Furthermore, the generation of maximally entangled W-states was also demonstrated theoretically by postselecting events at equal detection times at the output of a tritter for photons of completely different colors [5].

It was also shown that the access to the quantum information encoded in the spectra of the interfering photons via correlation measurements in the photonic inner degrees of freedom can unravel the full classical hardness of multiphoton interference in boson sampling schemes [18, 19]. This is even the case if no overlap between the input photon frequency and temporal spectra occurs [19, 39, 40]. Furthermore, it is possible to generate a boson sampling input state in an approximately deterministic way with photons of random spectral overlap and/or with random occupation numbers at the input [41].

Despite all these remarkable results, the full quantum advantages of multiphoton interference based on inner-mode resolved linear optics arising in quantum optics experiments even beyond boson sampling are still far from being fully explored. In particular, working towards novel schemes for the characterization of multiphoton networks and entanglement generation with nonidentical photons, important questions arise:

a) How can given symmetries in the multiphoton input state and in its evolution in a linear optical network be inferred from the measurement of inner-mode correlations at the network output? b) How do time and frequency resolved measurements tailor the type of entanglement correlations at the output of a linear network depending on the photonic input spectra?

By tackling these fundamental questions, we demonstrate in this paper how the full set of outcomes of inner-mode resolved measurements of a small number of nonidentical input photons in a linear optical network allows one to: a) infer information about symmetries of optical networks and of multiphoton quantum states; b) mea-

* vincenzo.tamma@port.ac.uk

sure arbitrary degrees of W-state entanglement of a given small number of photons with a fixed configuration of the linear optical network. Remarkably, these results apply to photons of either different colors or injection times, dramatically increasing the number of possible sources that can be exploited for future experiments (e.g. quantum dots).

II. MULTIPHOTON CORRELATIONS IN LINEAR NETWORKS

All of the experimental scenarios described in this paper are based on the N-photon linear optical networks depicted in Fig. 1 with $M \geq N$ ports $s = 1, 2, ..., M$.

Contrary to conventional multiphoton linear optical networks, N input single photons

$$|1; \xi_s, \omega_s, t_s\rangle_s \coloneqq \int_0^\infty d\omega\, \xi_s(\omega - \omega_s)\, \mathrm{e}^{+\mathrm{i}\omega t_s}\, \hat{a}_s^\dagger(\omega)|0\rangle_s \quad (1)$$

with nonidentical normalized spectra $\xi_s(\omega-\omega_s)\,\mathrm{e}^{\mathrm{i}\omega t_s}$, differing either in their injection times $\{t_s\} \coloneqq \{t_s \in \mathbb{R} \mid s \in \mathcal{S}\}$ or in their central frequencies $\{\omega_s\} \coloneqq \{\omega_s \in \mathbb{R}^+ \mid s \in \mathcal{S}\}$, are injected in a set $\mathcal{S}$ of N input ports, leading to the overall input state

$$|\psi_{\mathrm{in}}\rangle \coloneqq \bigotimes_{s\in\mathcal{S}} |1; \xi_s, \omega_s, t_s\rangle_s \bigotimes_{s\notin\mathcal{S}} |0\rangle_s. \quad (2)$$

For simplicity, we assume that the spectra of the input photons satisfy the narrow bandwidth approximation $\Delta\omega_s \ll \omega_s$, with the single-photon bandwidths $\Delta\omega_s$, and a polarization-independent interferometric evolution. Furthermore, given an overall frequency spread $\Delta\omega_{\mathrm{tot}}$ of the input light, we assume that all possible paths through the network are equal on the scale of the coherence length $c/\Delta\omega_{\mathrm{tot}}$. In this case, the interferometric evolution is also frequency independent (see App. A for details) and can be described by a single unitary $M \times M$ matrix $\mathcal{U}$ which defines the linear transformation

$$\hat{a}_d(\omega) = \sum_{s=1}^{M} \mathcal{U}_{ds} \hat{a}_s(\omega) \quad (3)$$

between the mode operators $\hat{a}_d(\omega)$ and $\hat{a}_s(\omega)$ at the output and input of the network, respectively.

The N photons are subsequently detected in a subset $\mathcal{D}$ containing N of the output ports $d = 1, \ldots, M$ and at frequencies $\{\omega_d\} \coloneqq \{\omega_d \in \mathbb{R}^+ \mid d \in \mathcal{D}\}$ or at times $\{t_d\} \coloneqq \{t_d \in \mathbb{R} \mid d \in \mathcal{D}\}$. Indeed, these measurements "erase" the distinguishability of the input photons in the respective conjugate photonic inner parameters: If the photons are distinguishable in frequency, multiphoton indistinguishability at the output of the network is ensured by a small enough detector integration in time [5, 19]

$$\delta t \ll 1/\Delta\omega_{\mathrm{tot}},$$

while a high frequency resolution

$$\delta\omega \ll |t_s - t_{s'}|^{-1}\ \forall s, s' \in \mathcal{S} \quad \text{and} \quad \delta\omega \ll \Delta\omega_s\ \forall s \in \mathcal{S}$$

ensures the indistinguishability of photons injected at different times [41].

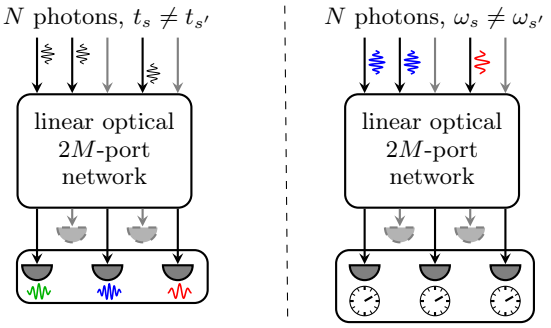

a) frequency-resolved detections b) time-resolved detections

Figure 1. a) Setup for frequency-resolved correlation measurements: N single photons, with generally different but overlapping frequency distribution ξ_s, are injected at different times $t_s \neq t_{s'}$ $(s, s' \in \mathcal{S})$ into a subset $\mathcal{S}$ of the input ports of a passive linear network and detected using frequency-resolving detectors. b) Setup for time-resolved correlation measurements: N single photons with different central frequencies $\omega_s \neq \omega_{s'}$ but overlapping temporal distributions $\mathcal{F}[\xi_s]$ are injected into a passive linear network and detected using time-resolving detectors.

In order to emphasize that our results apply to both time and frequency resolved detection schemes due to the conjugacy of time and frequency, we will from here on use the following notation: The *inner-mode parameter* measured at detector d will be denoted as β_d ($\beta_d = t_d$ or $\beta_d = \omega_d$ for time or frequency resolved detection, respectively) while the conjugate inner-mode parameter in which the photons are distinguishable at the input ports s in Eq. (2) will be labeled as α_s ($\alpha_s = \omega_s$ or $\alpha_s = t_s$ for time or frequency resolved detection, respectively).

The detection probability at the output at frequencies or times $\beta_d = \omega_d, t_d$ for input photons of different central times or frequencies $\alpha_s = t_s, \omega_s$, respectively, can be easily expressed in terms of the bosonic mode operators

$$\hat{a}_d(\beta_d) = \begin{cases} \hat{a}_d(\omega_d) & \beta_d = \omega_d \\ \dfrac{1}{\sqrt{2\pi}} \displaystyle\int d\omega\, \hat{a}_d(\omega)\, \mathrm{e}^{-\mathrm{i}\omega t_d} & \beta_d = t_d \end{cases}$$

at the output channels as [5]

$$P^{(\mathcal{D},\mathcal{S})}_{\{\beta_d\},\{\alpha_s\}} = \langle\psi_{\mathrm{in}}| \prod_{d\in\mathcal{D}} \hat{a}_d^\dagger(\beta_d) \prod_{d\in\mathcal{D}} \hat{a}_d(\beta_d)\, |\psi_{\mathrm{in}}\rangle.$$

Using the notation $\||\psi\rangle\|^2 \coloneqq \langle\psi|\psi\rangle$ and Eq. (3), this can be expressed in terms of the mode operators $\hat{a}_s(\beta_d)$ at the input channels as

$$P^{(\mathcal{D},\mathcal{S})}_{\{\beta_d\},\{\alpha_s\}} = \left\| \sum_{s_1,\ldots,s_N=1}^{N} \prod_{d\in\mathcal{D}} \mathcal{U}_{ds_d} \hat{a}_{s_d}(\beta_d)|\psi_{\mathrm{in}}\rangle \right\|^2.$$

Due to the structure of the state $|\psi_{\text{in}}\rangle$ in Eq. (2), only those terms contribute in which each of the N annihilation operators $\hat{a}_s(\beta)$, $s \in \mathcal{S}$, appears exactly once. Furthermore,

$$\hat{a}_s(\beta)|1;\xi_s,\omega_s,t_s\rangle_s = f_s(\beta-\beta_s)\,\mathrm{e}^{\mathrm{i}\beta\alpha_s}|0\rangle,$$

where we defined $f_s(\beta_d-\beta_s)=\xi_s(\omega_d-\omega_s)$ for frequency resolved detection or $f_s(\beta_d-\beta_s)=\mathcal{F}[\xi_s](t_d-t_s)$ for time resolved detection ($\mathcal{F}[\xi_s]$ is the Fourier transform of the frequency distribution ξ_s). Consequently, the inner-mode resolved correlations can be cast into the final form

$$P^{(\mathcal{D},\mathcal{S})}_{\{\beta_d\},\{\alpha_s\}} = \left|\sum_{\sigma}\prod_{d\in\mathcal{D}} \mathcal{U}_{d\sigma(d)} f_{\sigma(d)}(\beta_d-\beta_{\sigma(d)})\,\mathrm{e}^{\mathrm{i}\beta_d\alpha_{\sigma(d)}}\right|^2, \tag{4}$$

where the sum runs over all possible multiphoton paths σ (permutations from the symmetric group of order N) which bijectively connect the output ports $\mathcal{D}$ with the input ports $\mathcal{S}$.

The probabilities in Eq. (4) are the result of the interference between $N!$ multiphoton probability amplitudes each corresponding to one of the possible multiphoton quantum paths from the sources to the detectors [5, 39]. These amplitudes are not only determined by the linear network but also depend on the state of the input photons and on the detected frequencies or times, leading to quantum beating of the coincidence probabilities if the conjugate initial inner-mode values $\{\alpha_s\}$ are distinct. The additional dependence of the correlations on the detected inner-mode values is a manifestation of the increased information accessible by inner-mode resolved detections. This information can be employed as a quantum resource to unravel symmetry structures in multiphoton interference patterns as well as to tailor non-local multiphoton correlations.

III. SYMMETRIES OF INNER-MODE RESOLVED CORRELATIONS

We show how symmetries in the interference pattern of the correlations in the photonic inner modes described by Eq. (4) provide a tool to reveal information about the N-photon states, their interferometric evolution, or both simultaneously. Indeed, each N-photon interference amplitude in these correlations is given by the product of an interferometric amplitude

$$\mathcal{A}_\sigma \coloneqq \prod_{d\in\mathcal{D}} \mathcal{U}_{d\sigma(d)}$$

and a spectral amplitude

$$\begin{aligned}\mathcal{B}_\sigma(\{\beta_d\}) &= \mathcal{B}_\sigma(\{\beta_d\};\{f_s\},\{\alpha_s\},\{\beta_s\}) \\ &\coloneqq \prod_{d\in\mathcal{D}} f_{\sigma(d)}(\beta_d-\beta_{\sigma(d)})\,\mathrm{e}^{\mathrm{i}\beta_d\alpha_{\sigma(d)}}\,.\end{aligned} \tag{5}$$

To investigate the symmetry properties of the N-photon detection probability in Eq. (4), we consider its behaviour under an arbitrary linear transformation $\mathcal{T}:\{\beta_d\}\to \mathrm{span}(\{\beta_d\})^{\otimes N}$ of its inner-mode arguments β_d leading to

$$P^{(\mathcal{D},\mathcal{S})}_{\mathcal{T}(\{\beta_d\}),\{\alpha_s\}} = \left|\sum_{\sigma}\mathcal{A}_\sigma\mathcal{B}_\sigma\big(\mathcal{T}(\{\beta_d\})\big)\right|^2. \tag{6}$$

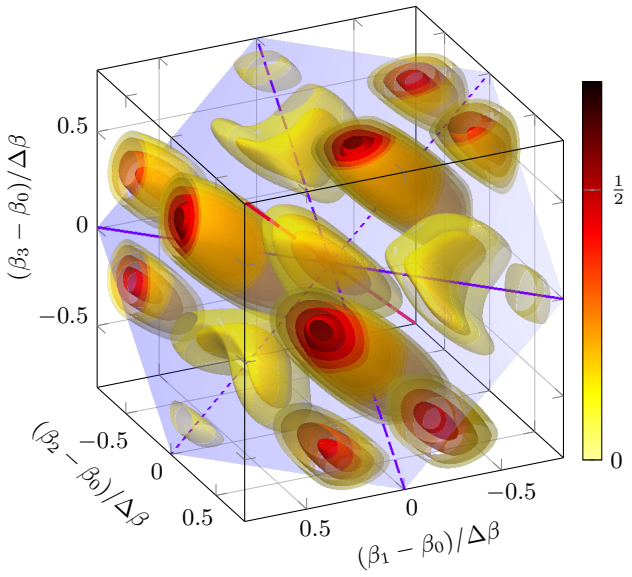

Figure 2. The inner-mode resolved interference pattern defined by Eq. (4) at the output of a symmetric tritter for three photons with input parameters $\{\alpha_s\}=\{0,7.4/\Delta\beta,11.3/\Delta\beta\}$ ($\alpha_s=t_s,\omega_s$) and equal Gaussian distributions $f(\beta_d-\beta_0)$ of bandwidth $\Delta\beta$, centered at β_0 ($\beta_d=\omega_d,t_d$). The behaviour of the multiphoton interference pattern under permutations τ of the detected inner-mode values β_d reveals two distinct classes of symmetries: a) a threefold rotational symmetry around the axis $(1,1,1)$ [—] if τ is (1)(2)(3) [rotation by 0°], (123) [120°], or (132) [240°], arising uniquely from the symmetric tritter, described by Eq. (13); b) three twofold rotational symmetry axes which correspond to τ being (12)(3) [—], (23)(1) [- -], or (13)(2) [···], emerging from a combination of the network's symmetry and a symmetry of the input frequency distributions around a common central frequency, described by Eq. (14). Lastly, a symmetry plane (light blue) orthogonal to the axis $(1,1,1)$ exists due to the highly symmetric input state of the photons (equal Gaussian inner-mode distributions), independently of the unitary transformation incurred by the linear network.

A. General photon numbers

a. Spectral symmetries. As a first example, we address the case where the multiphoton spectral amplitude $\mathcal{B}_\sigma$ defined by the spectra of the input photons is symmetric under a given transformation $\mathcal{T}$ apart from a permutation-independent phase $\phi(\{\beta_d\})$, i.e.

$$\mathcal{B}_\sigma\big(\mathcal{T}(\{\beta_d\})\big) = \mathrm{e}^{\mathrm{i}\phi(\{\beta_d\})}\,\mathcal{B}_\sigma(\{\beta_d\}). \tag{7}$$

In this case also the correlations in Eq. (6) manifest the same symmetry. Therefore, symmetric properties of the

input temporal and frequency spectra can be revealed from the measured symmetries of the multiphoton interference pattern independently of the optical network.

For example, the correlation probability in Eq. (6) is invariant under an inversion $\mathcal{T}_{\hat{\mathbf{n}}}$ of the landscape along the direction $\hat{\mathbf{n}} = (1, \dots, 1)^T$ where $\beta_1 = \beta_2 = \cdots = \beta_N$ if the input photons all exhibit the same Gaussian distribution centered at the frequency or time $\beta_0 = \omega_0, t_0$, respectively. Indeed, in this case the product $\prod_d f_{\sigma(d)}(\beta_d - \beta_0)$ in Eq. (5) only depends on the sum $\sum_d (\beta_d - \beta_0)^2$ and is consequently invariant under the unitary transformation

$$\mathcal{T}_{\hat{\mathbf{n}}} : \beta_d - \beta_0 \mapsto \beta_d - \beta_0 - \frac{2}{N} \sum_{d' \in \mathcal{D}} (\beta_{d'} - \beta_0). \tag{8}$$

Furthermore, the total phase of the term $\prod_d \exp(\mathrm{i}\beta_d \alpha_{\sigma(d)})$ in Eq. (5) transforms as

$$\sum_{d \in \mathcal{D}} \beta_d \alpha_{\sigma(d)} \overset{\mathcal{T}_{\hat{\mathbf{n}}}}{\mapsto} \sum_{d \in \mathcal{D}} \beta_d \alpha_{\sigma(d)} - \frac{2}{N} \sum_{s \in \mathcal{S}} \alpha_s \sum_{d' \in \mathcal{D}} (\beta_{d'} - \beta_0)$$

according to Eq. (8), where the second term is independent of the quantum path σ. Together with the invariance of $\prod_d f_{\sigma(d)}(\beta_d - \beta_0)$ this quantum path independent phase implies the symmetry of the spectral amplitudes as in Eq. (7) and therefore of the probabilities in Eq. (6), i.e.

$$P^{(\mathcal{D},\mathcal{S})}_{\mathcal{T}_{\hat{\mathbf{n}}}(\{\beta_d\}),\{\alpha_s\}} = P^{(\mathcal{D},\mathcal{S})}_{\{\beta_d\},\{\alpha_s\}}. \tag{9}$$

b. Parity symmetries. As a second example, we consider photonic input spectral distributions $f_s(\beta_d - \beta_0)$ in general different but symmetric around a common value β_0. In this case, the parity transformation

$$\mathcal{T}_{\mathrm{P}} : \beta_d - \beta_0 \mapsto -(\beta_d - \beta_0) \tag{10}$$

of the detected inner-mode values β_d is equivalent to the complex conjugation

$$\begin{aligned} \mathcal{B}_\sigma\big(\mathcal{T}_{\mathrm{P}}(\{2\beta_0 - \beta_d\})\big) &= \prod_{d \in \mathcal{D}} f_{\sigma(d)}(\beta_d - \beta_0)\, \mathrm{e}^{\mathrm{i}(2\beta_0 - \beta_d)\alpha_{\sigma(d)}} \\ &= \mathrm{e}^{\mathrm{i}2\beta_0 \sum_s \alpha_s}\, \mathcal{B}^*_\sigma(\{\beta_d\}) \end{aligned} \tag{11}$$

of the spectral multiphoton amplitudes defined in Eq. (5), apart from a phase term independent of the permutation σ. If additionally the unitary interferometer transformation is characterized by multiphoton amplitudes $\mathcal{A}_\sigma = \mathcal{A}^*_\sigma\, \mathrm{e}^{\mathrm{i}\varphi}$ with the same complex phase φ, the measured multiphoton interference pattern

$$\begin{aligned} P^{(\mathcal{D},\mathcal{S})}_{\mathcal{T}_{\mathrm{P}}(\{\beta_d\}),\{\alpha_s\}} &= \Big|\sum_\sigma \mathcal{A}_\sigma \mathcal{B}^*_\sigma(\{\beta_d\})\Big|^2 \\ &= \Big|\sum_\sigma \mathrm{e}^{\mathrm{i}\varphi}\, \mathcal{A}^*_\sigma \mathcal{B}^*_\sigma(\{\beta_d\})\Big|^2 = P^{(\mathcal{D},\mathcal{S})}_{\{\beta_d\},\{\alpha_s\}} \end{aligned}$$

is invariant under the transformation Eq. (10). We emphasize that this parity symmetry occurs independently of the linear network if the inner-mode values α_s are identical.

c. Permutation symmetries. As a final example, we consider the case of a permutation τ of the inner-mode arguments in Eq. (6) corresponding to the transformation

$$\mathcal{T}_\tau : \beta_d \mapsto \beta_{\tau(d)}.$$

By reordering the product defining the spectral amplitude in Eq. (5), the transformed spectral amplitudes can be recast to

$$\begin{aligned} \mathcal{B}_\sigma(\mathcal{T}\{\beta_{\tau(d)}\}) &= \prod_{d \in \mathcal{D}} f_{\sigma(d)}(\beta_{\tau(d)} - \beta_{\sigma(d)})\, \mathrm{e}^{\mathrm{i}\beta_{\tau(d)}\alpha_{\sigma(d)}} \\ &= \prod_{d \in \mathcal{D}} f_{\sigma(\tau^{-1}(d))}(\beta_d - \beta_{\sigma(\tau^{-1}(d))})\, \mathrm{e}^{\mathrm{i}\beta_d \alpha_{\sigma(\tau^{-1}(d))}} \\ &= \mathcal{B}_{\sigma\circ\tau^{-1}}(\{\beta_d\}), \end{aligned}$$

where $\circ$ denotes the concatenation of permutations. Consequently,

$$\begin{aligned} P^{(\mathcal{D},\mathcal{S})}_{\{\beta_{\tau(d)}\},\{\alpha_s\}} &= \Big|\sum_\sigma \mathcal{A}_{\sigma\circ\tau} \mathcal{B}_{\sigma\circ\tau^{-1}}(\{\beta_d\})\Big|^2 \\ &= \Big|\sum_\sigma \mathcal{A}_{\sigma\circ\tau} \mathcal{B}_\sigma(\{\beta_d\})\Big|^2, \end{aligned} \tag{12}$$

i.e. a permutation of the values β_d can be mapped to a permutation of the interferometric amplitudes $\mathcal{A}_\sigma$. Interestingly, this implies that some symmetries in the measured inner-mode resolved correlations can be intrinsically connected to symmetries in the interferometric amplitudes. Namely, if $\mathcal{A}_{\sigma\circ\tau} = \mathcal{A}_\sigma\, \mathrm{e}^{\mathrm{i}\varphi}\, \forall\sigma$ with a phase φ for a given permutation τ the interference pattern is symmetric under the corresponding permutation of the detected parameters $\{\beta_d\}$,

$$P^{(\mathcal{D},\mathcal{S})}_{\{\beta_{\tau(d)}\},\{\alpha_s\}} = P^{(\mathcal{D},\mathcal{S})}_{\{\beta_d\},\{\alpha_s\}}. \tag{13}$$

Furthermore, in the case where $\mathcal{A}_{\sigma\circ\tau} = \mathcal{A}^*_\sigma\, \mathrm{e}^{\mathrm{i}\varphi}\, \forall\sigma$, we find – using Eqs. (11) and (12) – that the correlations are symmetric under a combination of the permutation τ and the parity operation $\beta_d \to 2\beta_0 - \beta_d$,

$$P^{(\mathcal{D},\mathcal{S})}_{\{2\beta_0 - \beta_{\tau(d)}\},\{\alpha_s\}} = P^{(\mathcal{D},\mathcal{S})}_{\{\beta_d\},\{\alpha_s\}}, \tag{14}$$

if the spectral distributions are all symmetric around the same central value β_0.

We emphasize that the symmetries described here are encoded in the inner-mode resolved interference pattern. If no inner-mode resolved measurements are employed these structures cannot be observed and the corresponding symmetries cannot be retrieved [5, 42].

Even though the number of measurements necessary to reconstruct the full interference pattern increases exponentially with the number of photons in the present formulation, this technique can surely be applied for experiments with low photon numbers.

B. Example: Three-photon symmetries

In order to provide a practical example of some of the symmetric properties described so far, we consider the case of three photons with identical spectral distributions $f(\beta_d - \beta_0)$ but different injection times or central frequencies $\alpha_s = t_s, \omega_s$ measured at the output of a symmetric tritter at frequencies $\beta_d = \omega_d$ or times $\beta_d = t_d$, respectively. The corresponding correlations depicted in Fig. 2 depicted as a function of the detected inner-mode parameters $\{\beta_d\}$ exhibit not only three-photon quantum beating [5] but also several evident symmetries in the measured photonic inner parameters. We will now describe how these symmetries originate from either the interferometer transformation $\mathcal{U}$, or the input state, or a combination of both.

a. Permutation symmetries. We first find from the symmetric tritter single-photon amplitudes $\mathcal{U}_{ds} := \exp(\mathrm{i}\frac{2\pi}{3}ds)/\sqrt{3}$ $(d, s = 1, 2, 3)$ that $\mathcal{A}_{\sigma\circ\tau} = \mathcal{A}_\sigma$ if the permutation τ is either (1)(2)(3), (123), or (132) [using cycle notation of permutations] and consequently that the probability remains unchanged under these permutations of the inner-mode variables β_d, as is clear from the result for arbitrary values of N in Eq. (13). As depicted in Fig. 2, this results in a threefold rotational symmetry axis (red line) emerging solely from the symmetry of the linear optical network. We understand this by noting that the permutation (123) acting onto the vector $(\beta_1, \beta_2, \beta_3)$ corresponds to a permutation matrix

$$R_{(123)} = \begin{pmatrix} 0 & 1 & 0 \\ 0 & 0 & 1 \\ 1 & 0 & 0 \end{pmatrix},$$

which at the same time represents a rotation of 240° around the axis $\beta_1 = \beta_2 = \beta_3$. Consequently, $\tau = (123)$ yields a rotation of the correlation pattern itself $-240°$ or equivalently 120°. Equivalently, the permutation (132) corresponds to a rotation by 240° around the same axis.

A second class of symmetries correspond to the permutations (12)(3), (23)(1), or (13)(2) for which $\mathcal{A}_{\sigma\circ\tau} = \mathcal{A}^*_\sigma$. According to Eq. (14), these correlations are symmetric under a combination of these permutations with a parity operation, given a symmetry of the inner-mode distributions of the input photons around a common value of the central inner-mode parameter $\beta_0 = \omega_0, t_0$. These symmetries show up as three distinct twofold rotational symmetry axes in Fig. 2 (blue lines). For example, the permutation (12)(3) together with the parity operation is represented by the negative permutation matrix

$$-R_{(12)(3)} = \begin{pmatrix} 0 & -1 & 0 \\ -1 & 0 & 0 \\ 0 & 0 & -1 \end{pmatrix}$$

which is equivalent to a rotation by 180° around the axis $\nu_1 + \nu_2 = 0, \nu_3 = 0$ (solid blue line in Fig. 2). The two remaining permutations (23)(1) and (13)(2) are analogously connected to twofold rotational symmetries around the axes defined by $\nu_2 + \nu_3 = 0, \nu_1 = 0$ (dashed blue line) or by $\nu_1 + \nu_3 = 0, \nu_2 = 0$ (dotted blue line), respectively.

b. Mirror symmetry. Finally, the choice of a highly symmetric input state (three photons with identical Gaussian distributions) leads to a symmetry under the linear transformation $\mathcal{T}_{\hat{\mathbf{n}}}$ in Eq. (8). Namely, in the three-photon case considered here, Eq. (9) corresponds to a mirror symmetry with respect to the blue plane orthogonal to the axis $(1, 1, 1)$ in Fig. 2. The combination of this mirror symmetry with the rotational symmetries corresponding to the permutations (12)(3), (23)(1), and (13)(2) leads to three distinct mirror symmetries, each corresponding to a mirror plane spanned by the red axis and one of the blue axes.

c. Parity symmetry. We also notice that no parity invariance arises in the interference pattern in Fig. 2 since the multiphoton amplitudes $\mathcal{A}_\sigma$ do not have the same complex phase and therefore do not satisfy the condition pointed out before for parity invariance.

IV. MULTIPHOTON ENTANGLEMENT FEATURES

Remarkably, inner-mode correlation measurements also allow us to encode a whole family of entangled N-qubit states in the outcomes of the measurements. In particular, we will show how entanglement in the polarization modes can be tailored depending on the inner-mode input parameters α_s and the detected conjugate parameters β_d. For this purpose, we generalize the photonic input state $|\psi_{\mathrm{in}}\rangle$ in Eq. (1) to describe N photonic qubits with horizontal (H) or vertical (V) polarization as

$$|1; \xi_s, \omega_s, t_s, \lambda_s\rangle_s := \int_0^\infty d\omega\, \xi_s(\omega - \omega_s)\, \mathrm{e}^{+\mathrm{i}\omega t_s}\, \hat{a}^\dagger_{s,\lambda_s}(\omega)|0\rangle_s,$$

with $\lambda_s = \mathrm{H}, \mathrm{V}$. Then, inner-mode correlation measurements at the output of a generalised symmetric beam splitter – described by the unitary $\mathcal{U}_{ds} = \exp(\mathrm{i}\frac{2\pi}{N}ds)/\sqrt{N}$ and assumed to be polarization independent – can lead to entanglement correlations spanning the full class of N-qubit W-states [43]. This can be achieved by choosing $N-1$ H- and one V-polarized photons ($\lambda_1 = \cdots = \lambda_{N-1} = \mathrm{H}, \lambda_N = \mathrm{V}$) with identical frequency distribution $\xi(\omega)$ as the input state

$$|\psi_{\mathrm{in}}\rangle = \bigotimes_{s=1}^{N-1} |1; \xi, \omega_s, t_s, \mathrm{H}\rangle_s |1; \xi, \omega_s, t_s, \mathrm{V}\rangle_N.$$

By rewriting the creation operators $\hat{a}^\dagger_{s,\lambda_s}$ at the input as the linear combination

$$\hat{a}^\dagger_{s,\lambda_s}(\beta) = \sum_d \mathcal{U}_{ds} \hat{a}^\dagger_{d,\lambda_s}(\beta)$$

of the creation operators $\hat{a}^\dagger_{d,\lambda_s}$ at the output in analogy to Eq. (3), the state $|\psi_{\mathrm{in}}\rangle$ can be propagated to the output

of the interferometer. The resulting output state

$$|\psi_{\text{out}}\rangle = \prod_{s=1}^{N}\sum_{d_s=1}^{N}\mathcal{U}_{d_s s}\int d\beta_s\, f_s(\beta_s)\,\mathrm{e}^{\mathrm{i}\beta_s\alpha_s}\,\hat{a}^{\dagger}_{d_s,\lambda_s}(\beta_s)|0\rangle$$

contains contributions for all possible sets of output channels where the photons are found. However, an inner-mode resolved, N-fold coincidence measurement at the output of the network is only sensitive to the contribution

$$\begin{aligned}|\psi^{(1\ldots N)}_{\text{out}}\rangle &= \int d^N\beta_d \sum_{\sigma\in\Sigma_N}\mathcal{A}_\sigma\mathcal{B}_\sigma(\{\beta_d\})|\{\lambda_{\sigma(d)}\},\{\beta_d\}\rangle \\ &= \int d^N\beta_d \sum_{j=1}^{N}\Big[\sum_{\substack{\sigma\\ \sigma(j)=N}}\mathcal{A}_\sigma\mathcal{B}_\sigma(\{\beta_d\})\Big]|\underbrace{\mathrm{H}\ldots\mathrm{H}}_{j-1}\,\mathrm{V}\,\underbrace{\mathrm{H}\ldots\mathrm{H}}_{N-j},\{\beta_d\}\rangle\end{aligned} \tag{15}$$

corresponding to a single-photon being detected at each of the output channels. The second line in Eq. (15) reveals that the sum in this expression defines a state from the class of N-qubit W-states for any given set of detected inner-mode values $\{\beta_d\}$. Consequently, the setup described in this section can be employed to generate a whole class W-states of multiple qubits which are parametrized by the detected inner-mode values $\{\beta\}$.

Since such a scheme relies on postselecting only the detections events of one photon per output port, the probability of generating W-state correlations scales down exponentially with the number of photons. Nonetheless, the scheme can be used to observe entanglement between a low number of nonidentical photons.

A. Entanglement of three photons

We now consider the case of $N = 3$ as an example. Here, coincidences of all three detectors are sensitive to the state component

$$\begin{aligned}|\psi^{(123)}_{\text{out}}\rangle = \int d^3\beta_d \prod_{d=1}^{3} f(\beta_d)\Bigg[&\sum_{\sigma\in\{(13)(2),(132)\}}\mathcal{A}_\sigma\,\mathrm{e}^{\mathrm{i}\beta_d\alpha_{\sigma(d)}}|\mathrm{VHH},\{\beta_d\}\rangle \\ &+\sum_{\sigma\in\{(23)(1),(123)\}}\mathcal{A}_\sigma\,\mathrm{e}^{\mathrm{i}\beta_d\alpha_{\sigma(d)}}|\mathrm{HVH},\{\beta_d\}\rangle + \sum_{\sigma\in\{(12)(3),(1)(2)(3)\}}\mathcal{A}_\sigma\,\mathrm{e}^{\mathrm{i}\beta_d\alpha_{\sigma(d)}}|\mathrm{HHV},\{\beta_d\}\rangle\Bigg]\end{aligned} \tag{16}$$

according to Eq. (15). This explicit form nicely illustrates that the amplitudes of the W-states inside the square brackets are the result of the interference between the two H-polarized photons. For example, the amplitude of $|\mathrm{VHH},\{\beta_d\}\rangle$ is the coherent superposition of the two possible quantum paths for which the V-polarized photon is detected in the first output channel.

For a given set of measured values $\{\beta_d\}$, the polarization state of the photons in Eq. (16) corresponds to a three-photon W-state

$$|W_{\{\beta_d\},\{\alpha_s\}}\rangle \coloneqq a|\mathrm{HHV}\rangle + b|\mathrm{HVH}\rangle + c|\mathrm{VHH}\rangle, \tag{17}$$

with amplitudes $a = a_{\{\beta_d\},\{\alpha_s\}}$, $b = b_{\{\beta_d\},\{\alpha_s\}}$, $c = c_{\{\beta_d\},\{\alpha_s\}}$ parametrized by the detected inner-mode values $\{\beta_d\} = \{\omega_d\},\{t_d\}$ and the input values $\{\alpha_s\} = \{t_s\},\{\omega_s\}$, respectively. As we demonstrate in App. B, the absolute values are given by

$$\begin{aligned}|a| &= \Big|\cos\Big(\frac{1}{2}(\beta_2-\beta_3)(\alpha_1-\alpha_2)-\frac{2\pi}{3}\Big)\Big|,\\ |b| &= \Big|\cos\Big(\frac{1}{2}(\beta_1-\beta_3)(\alpha_1-\alpha_2)+\frac{2\pi}{3}\Big)\Big|,\\ |c| &= \Big|\cos\Big(\frac{1}{2}\big((\beta_1-\beta_3)-(\beta_2-\beta_3)\big)(\alpha_1-\alpha_2)-\frac{2\pi}{3}\Big)\Big|,\end{aligned} \tag{18}$$

apart from a common normalization constant. As discussed above, the moduli of these coefficients arise from the interference between the H-polarized photons and the degree of entanglement is therefore independent of the inner-mode parameter α_3 of the V-polarized photon. Indeed, if the two H-polarized photons are offset in their initial inner-mode parameters with respect to each other ($\alpha_1 - \alpha_2 \neq 0$), their interference manifests in a beating behavior of the coefficients a, b, c, independently of the photonic frequency distribution $\xi(\omega)$. This beating behavior is depicted in Fig. 3a) in the particular case $(\beta_1-\beta_3)(\alpha_1-\alpha_2) = -(\beta_2-\beta_3)(\alpha_1-\alpha_2)$ for which $|a| = |b|$. Therefore, the inner-mode measurements span the full family of three-photon W-states in Eq. (17) through the beating behavior of the corresponding weights in Eq. (18) as a function of the detected inner-mode values $\{\beta_d\}$ and the input inner-mode values $\alpha_1 - \alpha_2$. In this respect, the input values α_s can also be spanned experimentally via inner-mode multiplexing with N SPDC sources, independently of the output values $\{\beta_d\}$ [41].

It is straightforward to describe how these inner-mode correlation measurements tailor the W-state entanglement by measuring the pairwise entanglement between

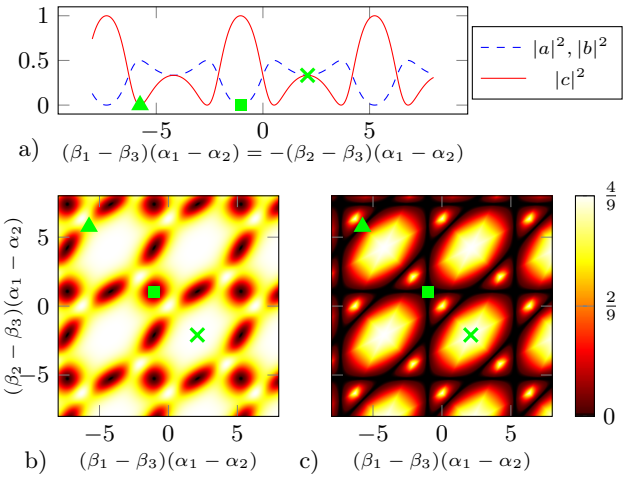

Figure 3. a) Beating in the probabilities $|a|^2$, $|b|^2$, $|c|^2$ defining the detected W-state in Eq. (17) generated by inner-mode resolved correlation measurements in the values $\beta_d = \omega_d, t_d$ of two H- and one V-polarized input photons of different parameters $\alpha_s = t_s, \omega_s$ at the output of a symmetric tritter. The inner-mode values β and α correspond to the frequency and time or vice versa. b) Average two-photon concurrence $E^{(\mathrm{av})}_{\{\beta_d\},\{\alpha_s\}}$ in Eq. (20). c) Minimum two-photon concurrence $E^{(\mathrm{min})}_{\{\beta_d\},\{\alpha_s\}}$ in Eq. (19). As an example, panel a) is plotted as a function of $(\beta_1-\beta_3)(\alpha_1-\alpha_2) = -(\beta_2-\beta_3)(\alpha_1-\alpha_2)$, corresponding to the antidiagonal of panels b) and c). Any degree of entanglement of the W-state class emerges from the beating of the amplitudes a, b, c caused by a difference in the input inner-mode parameters of the H-polarized photons ($\alpha_1 \neq \alpha_2$) when measurements in the conjugate parameters β_d are performed. As an example, tripartite entanglement of the W-state type, corresponding to the maximal possible value $E^{(\mathrm{av})} = E^{(\mathrm{min})} = 4/9$ [43], is uniquely achieved for $|a| = |b| = |c| = 1/\sqrt{3}$ (see cross mark as an example). Further, the detected state is fully separable when $E^{(\mathrm{av})} = E^{(\mathrm{min})} = 0$ since two of the amplitudes a, b, and c vanish (e.g. square mark). Last, a biseparable state is found when only one of the amplitudes vanishes (e.g. triangle mark). Such a state shows a high average entanglement $E^{(\mathrm{av})} = 1/3$ since two photons are maximally entangled, but a vanishing minimal entanglement $E^{(\mathrm{min})} = 0$ due to the biseparability.

the three possible photons pairs. This is possible since the tripartite entanglement of the W-state in Eq. (17) corresponds uniquely to the entanglement between all photon pairs. We will in the following quantify this pairwise entanglement in terms of the squared concurrences for each of the three possible reduced density matrices obtained by tracing the density matrix $\rho_{123} := |W_{\{\beta_d\},\{\alpha_s\}}\rangle\langle W_{\{\beta_d\},\{\alpha_s\}}|$ over output channel 1, 2, or 3, respectively [44].

The squared concurrence E_{12} of output channels 1 and 2 can for example be determined with the help of the matrix

$$R_{12} := \sqrt{\sqrt{\rho_{12}}(\sigma_y \otimes \sigma_y)\rho_{12}^*(\sigma_y \otimes \sigma_y)\sqrt{\rho_{12}}},$$

where σ_y denotes the Pauli matrix. Namely, labeling the eigenvalues of R_{12} as $\lambda_1 \geq \lambda_2 \geq \lambda_3 \geq \lambda_4$,

$$E_{12} := \left[\max(0, \lambda_1 - \lambda_2 - \lambda_3 - \lambda_4)\right]^2.$$

From these definitions, we find for the W-state in Eq. (17) that the squared concurrences can be expressed in terms of the amplitudes a, b, and c as (see [43])

$$E_{12} = 4|ab|^2; \quad E_{23} = 4|bc|^2; \quad E_{13} = 4|ac|^2.$$

By inserting the explicit form of the coefficients in Eqs. (18), these values can be expressed as functions of the detected inner-mode values at the output of the symmetric tritter.

The entanglement of the W-state is genuinely tripartite if the minimal squared concurrence [43]

$$\begin{aligned} E^{(\mathrm{min})}_{\{\beta_d\},\{\alpha_s\}} &:= \min\left(E_{12}, E_{23}, E_{13}\right) \\ &= 4\min\left(|ab|^2, |bc|^2, |ac|^2\right) \end{aligned} \tag{19}$$

is non-vanishing. If $E^{(\mathrm{min})}_{\{\beta_d\},\{\alpha_s\}} = 0$, the state is either 2- or 3-separable. These cases can be distinguished by the average squared concurrence

$$\begin{aligned} E^{(\mathrm{av})}_{\{\beta_d\},\{\alpha_s\}} &:= \frac{1}{3}\left(E_{12} + E_{23} + E_{13}\right) \\ &= \frac{4}{3}\left(|ab|^2 + |bc|^2 + |ac|^2\right). \end{aligned} \tag{20}$$

The state is 3-separable if $E^{(\mathrm{av})}_{\{\beta_d\},\{\alpha_s\}} = 0$ and 2-separable otherwise. Both $E^{(\mathrm{min})}_{\{\beta_d\},\{\alpha_s\}}$ and $E^{(\mathrm{av})}_{\{\beta_d\},\{\alpha_s\}}$ are maximized to the value 4/9 for a balanced W-state with $|a| = |b| = |c|$, yielding the bounds [43]

$$E^{(\mathrm{min})}_{\{\beta_d\},\{\alpha_s\}} \leq E^{(\mathrm{av})}_{\{\beta_d\},\{\alpha_s\}} \leq \frac{4}{9}.$$

The minimal and average squared concurrence are depicted in Fig. 3b) and 3c), respectively, as a functions of the relative detected inner-mode parameters $\{\beta_d\}$ and of the input inner-mode parameters $\alpha_1 - \alpha_2$. Evidently, the states encoded into the outcomes of the inner-mode measurements exhibit arbitrary degrees of tripartite entanglement of the W-state type from complete separability up to maximal entanglement (Fig. 3).

V. DISCUSSION

We have shown how frequency and time resolved multiphoton interference between nonidentical photons is a promising tool to unravel the symmetries characterizing

their quantum states and their evolution in linear optical networks. Exploiting inner-mode correlation measurements, the differences in the photonic inner-mode parameters (i.e. color or injection times), instead of being a challenge to overcome, become a powerful resource to generate entire families of W-states comprising a small number of photons with a single network. Indeed, this is possible by recording the inner-mode quantum information encoded in the interfering nonidentical photons. While the proposed schemes are not efficient in the present form for large photon numbers, they can be implemented for experimental realizations with low photon numbers. In particular, the experimental verification of the emergence of some of the multiphoton symmetries of optical networks predicted here has just recently been reported in Ref. [45].

In conclusion, these results have the potential to inspire novel platforms for the analysis of multiphoton linear networks and for multiphoton entanglement generation by employing the full quantum capabilities of inner-mode multiphoton interference in universal linear optics with arbitrary sources of nonidentical photons.

ACKNOWLEDGMENTS

The authors are grateful to C. Dewdney, K. Jacobs, S. Kolthammer, A. Laing, F. Sciarrino, and P. Walther for discussions related to this work.

Research was partially sponsored by the Army Research Laboratory and was accomplished under Cooperative Agreement Number W911NF-17-2-0179. The views and conclusions contained in this document are those of the authors and should not be interpreted as representing the social policies, either expressed or implied, of the Army Research Laboratory or the U.S. Government. The U.S. Government is authorized to reproduce and distribute reprints for Government purposes notwithstanding any copyright notation herein. V. T. is also thankful to W. P. Schleich for the time passed until the summer of 2016 at the Institute of Quantum Physics in Ulm where some of the ideas behind this work started to flourish. S. L. acknowledges support by a grant from the Ministry of Science, Research and the Arts of Baden-Württemberg (Az: 33-7533-30-10/19/2).

Both authors contributed equally to the obtained results. The project was conceived and managed by V.T.

Appendix A: Frequency-independence of linear network

In typical designs of linear optical networks, such as the ones used in experimental implementations of boson sampling, the beam splitters are located on a regular grid [46–48]. This ensures that the path lengths $\Delta x_{ds}^{(i)}$ of all possible paths through the interferometer are approximately equal to a given length Δx on the scale of the correlation length of the light, $\Delta x_{ds}^{(i)} = \Delta x + \delta x_{ds}^{(i)}$ with $|\delta x_{ds}^{(i)}| \ll 2\pi c/\Delta\omega_{\rm tot}$ $\forall i \forall s \forall d$ (i labels all possible paths connecting a fixed pair s, d of input and output channels). Consequently, by using the expression $\omega = \omega_0 + \Omega$ ($|\Omega| \leq \Delta\omega_{\rm tot}$) in terms of the overall central frequency ω_0, we obtain

$$\begin{aligned} \mathrm{e}^{\mathrm{i}\omega\Delta x_{ds}^{(i)}/c} &= \mathrm{e}^{\mathrm{i}\omega\Delta x/c + \mathrm{i}\omega_0\delta x_{ds}^{(i)}/c + \mathrm{i}\Omega\delta x_{ds}^{(i)}/c} \\ &\approx \mathrm{e}^{\mathrm{i}\omega\Delta x/c + \mathrm{i}\omega_0\delta x_{ds}^{(i)}/c}, \end{aligned}$$

since $|\Omega||\delta x_{ds}^{(i)}| \leq \Delta\omega_{\rm tot}|\delta x_{ds}^{(i)}| \ll c$. It immediately follows that the total probability amplitude connecting input channel s with output channel d can be written as

$$\begin{aligned} \mathcal{U}_{ds}(\omega) &= \sum_i \mathcal{U}_{ds}^{(i)}\, \mathrm{e}^{\mathrm{i}\omega\Delta x_{ds}^{(i)}/c} \\ &= \mathrm{e}^{\mathrm{i}\omega\Delta x/c} \sum_i \mathcal{U}_{ds}^{(i)}\, \mathrm{e}^{\mathrm{i}\omega_0\delta x_{ds}^{(i)}} = \mathcal{U}_{ds}\, \mathrm{e}^{\mathrm{i}\omega\Delta x/c}, \end{aligned}$$

where $\mathcal{U}_{ds} = \sum_i \mathcal{U}_{ds}^{(i)}\, \mathrm{e}^{\mathrm{i}\omega_0\delta x_{ds}^{(i)}}$. Without losing generality, we can set $\Delta x = 0$ since non-zero values only correspond to an offset of the detection times t_d.

Appendix B: W-state coefficients

According to Eq. (16), a three-fold coincidence event of the photons is sensitive only to the state component

$$|\psi_{\rm out}^{(123)}\rangle = \int d\beta_1 \int d\beta_2 \int d\beta_3 \prod_{d=1}^{3} f(\beta_d)\, \mathrm{e}^{\mathrm{i}\beta_3\alpha_d} \Big(\tilde{a}|\mathrm{VHH};\{\beta_d\}\rangle + \tilde{b}|\mathrm{HVH};\{\beta_d\}\rangle + \tilde{c}|\mathrm{HHV};\{\beta_d\}\rangle\Big),$$

with coefficients

$$\tilde{a} = \tilde{a}_{\{\beta_d\},\{\alpha_s\}} = \sum_{\sigma\in\{(13)(2),(132)\}} \mathcal{A}_\sigma\, \mathrm{e}^{\mathrm{i}\beta_d\alpha_{\sigma(d)}}$$

$$\tilde{b} = \tilde{b}_{\{\beta_d\},\{\alpha_s\}} = \sum_{\sigma\in\{(23)(1),(123)\}} \mathcal{A}_\sigma\, \mathrm{e}^{\mathrm{i}\beta_d\alpha_{\sigma(d)}}$$

$$\tilde{c} = \tilde{c}_{\{\beta_d\},\{\alpha_s\}} = \sum_{\sigma\in\{(12)(3),(1)(2)(3)\}} \mathcal{A}_\sigma\, \mathrm{e}^{\mathrm{i}\beta_d\alpha_{\sigma(d)}}$$

Inserting the interferometer multiphoton amplitudes $\mathcal{A}_\sigma$ for the symmetric tritter $\mathcal{U}_{ds} = \exp(\mathrm{i}2\pi ds/3)/\sqrt{3}$ the coefficient $\tilde{a}$ evaluates as

$$\tilde{a}_{\{\beta_d\},\{\alpha_s\}} = 3^{-3/2}\Big[\,\mathrm{e}^{-\mathrm{i}2\pi/3}\,\mathrm{e}^{\mathrm{i}\left((\beta_1-\beta_3)\alpha_3+(\beta_2-\beta_3)\alpha_1\right)} + \mathrm{e}^{+\mathrm{i}2\pi/3}\,\mathrm{e}^{\mathrm{i}\left((\beta_1-\beta_3)\alpha_3+(\beta_2-\beta_3)\alpha_2\right)}\,\Big].$$

Consequently, we arrive at

$$\tilde{a} = \tilde{a}_{\{\beta_d\},\{\alpha_s\}} = \frac{2}{3^{3/2}}\,\mathrm{e}^{\mathrm{i}(\beta_1-\beta_3)\alpha_3}\,\mathrm{e}^{\mathrm{i}\frac{1}{2}(\beta_2-\beta_3)(\alpha_1+\alpha_2)}\cos\left(\frac{1}{2}(\beta_2-\beta_3)(\alpha_1-\alpha_2)-\frac{2\pi}{3}\right) \tag{B1}$$

and the remaining coefficients analogously are

$$\tilde{b} = \tilde{b}_{\{\beta_d\},\{\alpha_s\}} = \frac{2}{3^{3/2}}\,\mathrm{e}^{\mathrm{i}\frac{1}{2}(\beta_1-\beta_3)(\alpha_1+\alpha_2)}\,\mathrm{e}^{\mathrm{i}(\beta_2-\beta_3)\alpha_3}\cos\left(\frac{1}{2}(\beta_1-\beta_3)(\alpha_1-\alpha_2)+\frac{2\pi}{3}\right)$$

$$\tilde{c} = \tilde{c}_{\{\beta_d\},\{\alpha_s\}} = \frac{2}{3^{3/2}}\,\mathrm{e}^{\mathrm{i}\frac{1}{2}((\beta_1-\beta_3)+(\beta_2-\beta_3))(\alpha_1+\alpha_2)}\cos\left(\frac{1}{2}((\beta_1-\beta_3)-(\beta_2-\beta_3))(\alpha_1-\alpha_2)-\frac{2\pi}{3}\right).$$

Since the coefficients only depend on the differences in the inner-mode values β_d we made the arbitrary choice to write them as functions of the pair of differences $\beta_1-\beta_3$ and $\beta_2-\beta_3$. Equivalently, we could have chosen $\beta_1-\beta_2$ and $\beta_3-\beta_2$ or $\beta_2-\beta_1$ and $\beta_3-\beta_1$.

The coefficients a, b, c of the W-state in Eq. (17) can be determined from Eq. (B1) by normalizing the coefficients $\tilde{a}, \tilde{b}, \tilde{c}$ with the factor $(|\tilde{a}|^2+|\tilde{b}|^2+|\tilde{c}|^2)^{-1/2}$.

[1] C. K. Hong, Z. Y. Ou, and L. Mandel, Phys. Rev. Lett. **59**, 2044 (1987).
[2] C. O. Alley and Y. H. Shih, in *Proceedings of the Second International Symposium on Foundations of Quantum Mechanics in the Light of New Technology* (Physical Soc. of Japan, Tokyo, 1986) pp. 47–52.
[3] Y. H. Shih and C. O. Alley, Phys. Rev. Lett. **61**, 2921 (1988).
[4] J.-W. Pan, Z.-B. Chen, C.-Y. Lu, H. Weinfurter, A. Zeilinger, and M. Żukowski, Rev. Mod. Phys. **84**, 777 (2012).
[5] V. Tamma and S. Laibacher, Phys. Rev. Lett. **114**, 243601 (2015).
[6] B. J. Metcalf, N. Thomas-Peter, J. B. Spring, D. Kundys, M. A. Broome, P. C. Humphreys, X.-M. Jin, M. Barbieri, W. S. Kolthammer, J. C. Gates, and others, Nature Commun. **4**, 1356 (2013).
[7] J. Carolan, C. Harrold, C. Sparrow, E. Martín-López, N. J. Russell, J. W. Silverstone, P. J. Shadbolt, N. Matsuda, M. Oguma, M. Itoh, Graham D. Marshall, Mark G. Thompson, Jonathan C. F. Matthews, Toshikazu Hashimoto, Jeremy L. O'Brien, and Anthony Laing, Science **349**, 711 (2015).
[8] F. Flamini, L. Magrini, A. S. Rab, N. Spagnolo, V. D'Ambrosio, P. Mataloni, F. Sciarrino, T. Zandrini, A. Crespi, R. Ramponi, and R. Osellame, Light Sci. Appl. **4**, e354 (2015).
[9] R. Hanbury Brown and R. Q. Twiss, Nature **178**, 1046 (1956).
[10] V. Tamma and S. Laibacher, Phys. Rev. A **90**, 063836 (2014).
[11] V. Tamma and J. Seiler, New J. Phys. **18**, 032002 (2016).
[12] M. Cassano, M. D'angelo, A. Garuccio, T. Peng, Y. Shih, and V. Tamma, Opt. Express **25**, 6589 (2017).
[13] T. Peng, V. Tamma, and Y. Shih, Sci. Rep. **6** (2016), 10.1038/srep30152.
[14] M. D'Angelo, A. Mazzilli, F. V. Pepe, A. Garuccio, and V. Tamma, Sci. Rep. **7** (2017), 10.1038/s41598-017-02236-8.
[15] T. D. Ladd, F. Jelezko, R. Laflamme, Y. Nakamura, C. Monroe, and J. L. O'Brien, Nature **464**, 45 (2010).
[16] J. D. Franson, Science **339**, 767 (2013).
[17] E. Knill, R. Laflamme, and G. J. Milburn, Nature **409**, 46 (2001), test.
[18] S. Aaronson and A. Arkhipov, in *Proceedings of the Forty-Third Annual ACM Symposium on Theory of Computing* (ACM, New York, 2011) pp. 333–342.
[19] S. Laibacher and V. Tamma, Phys. Rev. Lett. **115**, 243605 (2015).
[20] H.-K. Lo, M. Curty, and K. Tamaki, Nature Photon. **8**, 595 (2014).
[21] K. Mattle, H. Weinfurter, P. G. Kwiat, and A. Zeilinger, Phys. Rev. Lett. **76**, 4656 (1996).
[22] J. P. Dowling, Contemp. Phys. **49**, 125 (2008).
[23] G. B. Lemos, V. Borish, G. D. Cole, S. Ramelow, R. Lapkiewicz, and A. Zeilinger, Nature **512**, 409 (2014).
[24] W. Wasilewski, P. Kolenderski, and R. Frankowski, Phys. Rev. Lett. **99**, 123601 (2007).
[25] T. M. Babinec, B. J. M. Hausmann, M. Khan, Y. Zhang, J. R. Maze, P. R. Hemmer, and M. Lončar, Nat. Nanotechnol. **5**, 195 (2010).
[26] B. Lounis and W. E. Moerner, Nature **407**, 3 (2000).

[27] A. J. Shields, Nature Photon. **1**, 215 (2007).
[28] P. Michler, Science **290**, 2282 (2000).
[29] T. Legero, T. Wilk, M. Hennrich, G. Rempe, and A. Kuhn, Phys. Rev. Lett. **93**, 070503 (2004).
[30] M. Avenhaus, A. Eckstein, P. J. Mosley, and C. Silberhorn, Opt. Lett. **34**, 2873 (2009).
[31] A. O. C. Davis, P. M. Saulnier, M. Karpiński, and B. J. Smith, Opt. Express **25**, 12804 (2017).
[32] C. Polycarpou, K. N. Cassemiro, G. Venturi, A. Zavatta, and M. Bellini, Phys. Rev. Lett. **109**, 053602 (2012).
[33] T. Gerrits, F. Marsili, V. B. Verma, L. K. Shalm, M. Shaw, R. P. Mirin, and S. W. Nam, Phys. Rev. A **91**, 013830 (2015).
[34] R.-B. Jin, T. Gerrits, M. Fujiwara, R. Wakabayashi, T. Yamashita, S. Miki, H. Terai, R. Shimizu, M. Takeoka, and M. Sasaki, Opt. Express **23**, 28836 (2015).
[35] V. Shcheslavskiy, P. Morozov, A. Divochiy, Y. Vakhtomin, K. Smirnov, and W. Becker, Rev. Sci. Instrum. **87**, 053117 (2016).
[36] M. Grimau Puigibert, G. Aguilar, Q. Zhou, F. Marsili, M. Shaw, V. Verma, S. Nam, D. Oblak, and W. Tittel, Phys. Rev. Lett. **119**, 083601 (2017).
[37] S.-H. Tan, Y. Y. Gao, H. de Guise, and B. C. Sanders, Phys. Rev. Lett. **110**, 113603 (2013).
[38] H. de Guise, S.-H. Tan, I. P. Poulin, and B. C. Sanders, Phys. Rev. A **89**, 063819 (2014).
[39] V. Tamma and S. Laibacher, Quantum Inf. Process. **15**, 1241 (2015).
[40] V. Tamma, Int. J. Quantum Inf. **12**, 1560017 (2014).
[41] S. Laibacher and V. Tamma, arXiv preprint arXiv:1801.03832 (2018), arXiv:1801.03832.
[42] V. Tamma and S. Laibacher, J. Mod. Opt. **63**, 41 (2015).
[43] W. Dür, G. Vidal, and J. I. Cirac, Phys. Rev. A **62**, 062314 (2000).
[44] V. Coffman, J. Kundu, and W. K. Wootters, Phys. Rev. A **61**, 052306 (2000).
[45] X.-J. Wang, B. Jing, P.-F. Sun, C.-W. Yang, Y. Yu, V. Tamma, X.-H. Bao, and J.-W. Pan, Phys. Rev. Lett. **121**, 080501 (2018).
[46] M. Tillmann, B. Dakić, R. Heilmann, S. Nolte, A. Szameit, and P. Walther, Nature Photon. **7**, 540 (2013).
[47] T. Ralph, Nature Photon. **7**, 514 (2013).
[48] A. Crespi, R. Osellame, R. Ramponi, D. J. Brod, E. F. Galvão, N. Spagnolo, C. Vitelli, E. Maiorino, P. Mataloni, and F. Sciarrino, Nature Photon. **7**, 545 (2013).